Diamond & Related Materials 143 (2024) 110840

Contents lists available at ScienceDirect

Diamond & Related Materials

journal homepage: www.elsevier.com/locate/diamond

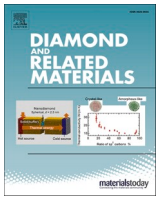

Highly efficient and atomic-scale smoothing of single crystal diamond through plasma-based atom-selective etching

Wang Liu [a,1], Yuxi Xiao [a,1], Yongjie Zhang [a,b], Quanpeng He [a], Hui Deng [a,*]

[a] Department of Mechanical and Energy Engineering, Southern University of Science and Technology, Shenzhen 518055, Guangdong, China
[b] Department of Physics and Centre for Advanced 2D Materials, National University of Singapore, 2 Science Drive 3, Singapore 117551, Singapore

ARTICLE INFO

Keywords:
SCD
PASE
ICP
Highly efficient smoothing
Atomic-scale smooth surface

ABSTRACT

Single crystal diamond (SCD) presents promising and extensive applications in electronics, thermal management, and optical windows for its excellent physical and chemical properties. However, its difficult-to-machine features, such as high hardness, processing brittleness, and chemical inertness make it challenging to smooth SCD, greatly inhibiting its further applications. Herein, a highly efficient and atomic-scale smoothing method for SCD based on the mechanism of plasma-based atom-selective etching (PASE) is proposed. During the smoothing process, oxygen active radicals in high temperature atmospheric inductively coupled plasma (ICP) would preferentially remove carbon atoms with more dangling bonds on SCD surface. By tuning the key parameters of oxygen plasma of radio frequency power, flow rate of oxygen, and torch-wafer distance, sufficient energy input and oxygen radicals concentration were obtained to generate PASE for SCD smoothing. The key parameters for PASE were investigated and the highest material removal rate reached up to 56.533 μm/min, which was thousands of times higher than conventional chemical mechanical polishing. After smoothing for 5 min, the *Sa* roughness began to stabilize at around 0.5 nm and an atomic-scale smooth surface was acquired. X-ray photoelectron spectroscopy, Raman spectroscopy, and transmission electron microscopy characterization results demonstrate that the smoothed SCD surface is crystallographically perfect without any non-diamond composition introduced. PASE of SCD with different initial surfaces, sizes, and crystal planes is proved to be feasible, showing the powerful applicability of PASE for SCD. In conclusion, PASE presents huge potential to achieve high-efficiency and atomic-scale smoothing of SCD to fulfill its industrial application demand.

1. Introduction

As one of the most precious mineral materials, single crystal diamond (SCD) possesses a series of excellent physical and chemical properties, showing promising and expansive applications in the field of engineering [1,2]. With the highest hardness, strong chemical inertness, and low friction coefficient, SCD has been widely used as cutting tools in ultra-precision manufacturing such as single point diamond turning [3,4]. Furthermore, SCD is also an ideal material for next-generation power semiconductor devices such as in Micro-Electro-Mechanical System (MEMS) due to its high breakdown field, thermal conductivity, and low dielectric constant compared with the traditional semiconductor materials, i.e., Si, 4H-SiC, GaN, and Ga_2O_3 [5]. Superior absorption band and high light transmittance characteristics make SCD have excellent performance when used as high-power infrared optical windows [6]. Additionally, SCD also shows attractive applications as electrically active components of bio-sensor for its excellent biocompatibility [7]. However, a large number of defects and damage on the diamond surface would directly affect the performance of SCD-based components, thereby deteriorating the quality factor of semiconductor devices, causing light scattering in optical application, increasing the friction coefficient of ultra-precision cutting tools, and reducing their service life [8–10]. Therefore, achieving a damage-free and atomic-scale smooth SCD surface is of great significance to promote its practical application.

SCD is a typical difficult-to-machine material due to its extreme mechanical hardness and chemical inertness. Nowadays, the widely adopted polishing method for SCD is mechanical polishing (MP). However, microcracks and subsurface damage can be easily introduced on the diamond surface during MP process. Even worse, the diamond substrate would crack if excessive pressure is applied through a scaife

* Corresponding author.
E-mail address: dengh@sustech.edu.cn (H. Deng).
[1] Authors contribute equally to this paper.

https://doi.org/10.1016/j.diamond.2024.110840
Received 12 November 2023; Received in revised form 15 January 2024; Accepted 15 January 2024
Available online 27 January 2024

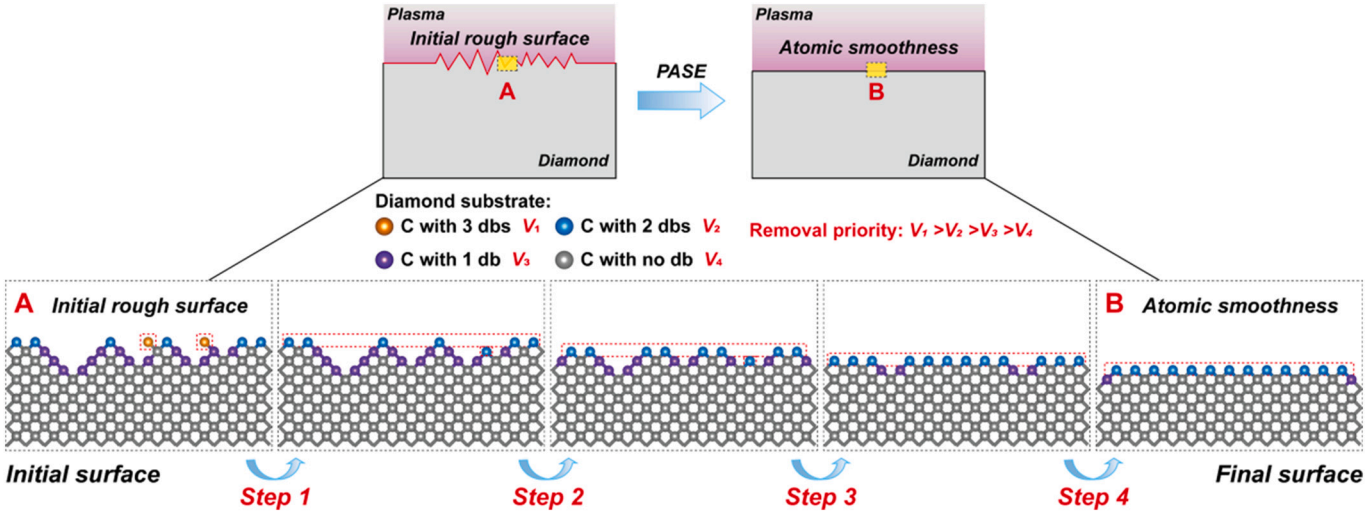

Fig. 1. Material removal mechanism of PASE of SCD. Carbon atoms marked with red dotted line would be removed preferentially. (For interpretation of the references to color in this figure legend, the reader is referred to the web version of this article.)

Table 1
Orthogonal experiments table of SCD.

Number	Factor 1	Factor 2	Factor 3	*Sa* (nm) (AFM 20 × 20 μm^2)
1	20 sccm	600 W	5 mm	0.605
2	20 sccm	800 W	15 mm	0.521
3	20 sccm	1000 W	10 mm	0.639
4	60 sccm	600 W	15 mm	105
5	60 sccm	800 W	10 mm	0.517
6	60 sccm	1000 W	5 mm	0.302
7	100 sccm	600 W	10 mm	0.759
8	100 sccm	800 W	5 mm	0.537
9	100 sccm	1000 W	15 mm	0.515

Table 2
Experimental parameters for different experiment schemes. (a) Experiment conditions for the exploration of the relation between MRR and each factor in orthogonal experiments. (b) Experiment conditions for smoothing of SCDs.

	Parameters	Conditions
(a)	Specimen	SCD (100) with 4 × 4 × 2 mm^3 dimensions
	RF power	600–1100 W
	RF frequency	27.12 MHz
	Carrier gas	Ar (1.5 slm)
	Reaction gas	O_2 (0–100 sccm)
	Cooling gas	Ar (18.0 slm)
	Quartz tube diameter	Inner tube: 14/16 mm inner/outer diameter Outer tube: 18/20 mm inner/outer diameter
	Torch-wafer distance	5–30 mm
	Parameters	Conditions
(b)	Specimen	SCD (100) with 4 × 4 × 2 mm^3 dimensions
	RF power	1000 W
	RF frequency	27.12 MHz
	Carrier gas	Ar (1.5 slm)
	Reaction gas	O_2 (20.0 sccm)
	Cooling gas	Ar (18.0 slm)
	Quartz tube diameter	Inner tube: 14/16 mm inner/outer diameter Outer tube: 18/20 mm inner/outer diameter
	Torch-wafer distance	15 mm

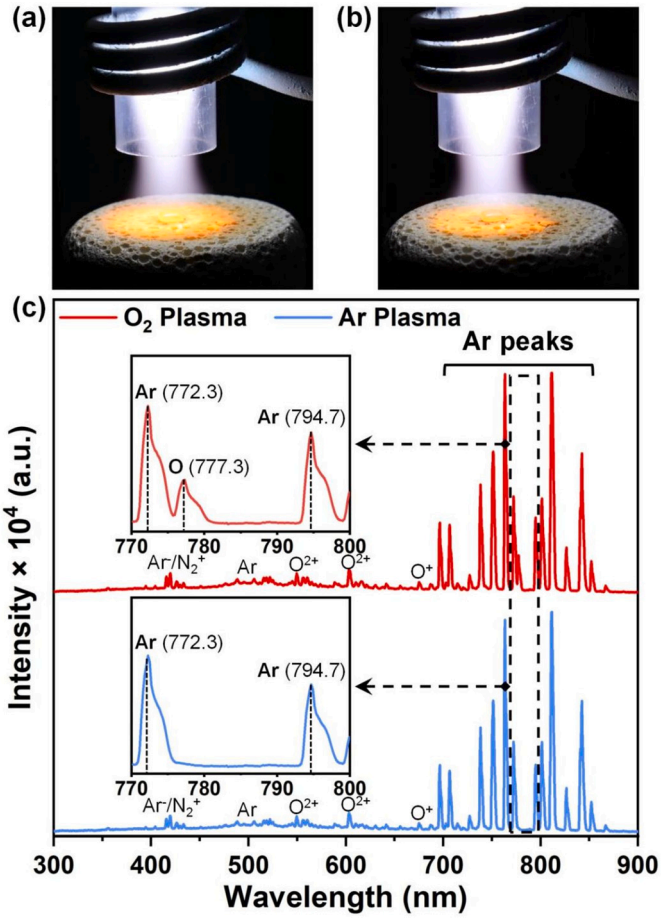

Fig. 2. Plasma excitation properties. (a) Oxygen plasma torch. (b) Pure argon plasma torch. (c) Optical emission spectroscopy of ICP.

which is a cast iron plate charged with diamond grits [11–13]. Additionally, the material removal rate (MRR) of diamond during MP is extremely low and it usually take a long time to polish in a specific orientation [14,15]. Chemical mechanical polishing (CMP) combines MP with chemical slurries to oxidize or modify the diamond surface, thereby softening surface removal layer. Compared with MP, CMP is more likely to realize considerate MRR and scratch-free diamond surface due to the lower polishing load. For CMP of SCD, chemical slurry takes a significant role in material removal process and extensive research has been done to explore a better polishing slurry. Yuan et al. explore slurries containing different oxidants found that the highest MRR of 0.055 mg/h and the best *Ra* roughness of 0.187 nm (atomic force microscopy (AFM), 10 × 10 μm^2) could be obtained by using K_2FeO_4 as the

Table 3
Estimates of level effects for factor 1 (flow rate of oxygen), factor 2 (RF power) and factor 3 (torch-wafer distance).

Estimate of level effect	Factor 1	Factor 2	Factor 3
I	1.765	106	1.445
II	106	1.575	1.915
III	1.811	1.456	106

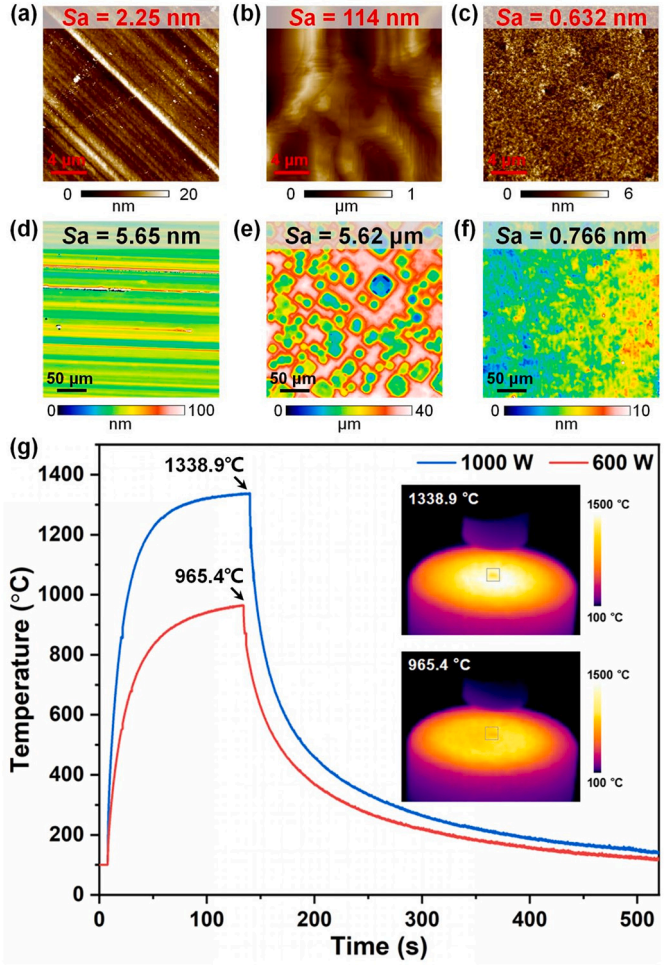

Fig. 3. Surface morphology and temperature characterization at different RF power. (a)–(c) AFM images of sample initial surface, surfaces after oxygen plasma treatment at 600 W and 1000 W, respectively. (d)–(f) SWLI images of sample initial surface, as well as surfaces after oxygen plasma treatment at 600 W and 1000 W. (g) Temperature profiles at different power.

oxidant [16]. Liao et al. also investigated slurries with different pH values and oxidants to polish SCD and obtained a surface with *Ra* roughness of 0.35 nm and MRR of 16.6 nm/h (3D optical surface profiler, 70 × 50 μm^2) by using the mixture of SiO_2, H_2O_2, $FeSO_4 \bullet 7H_2O$, and nitrilotriacetic acid [17]. Though the introduction of chemical reaction would improve the polishing efficiency and surface quality of diamond with a lower polishing load, it should be mentioned that the polishing efficiency is still too low for large-scale commercial application and the remaining contamination of slurry on the diamond surface would introduce extra post-treatment process. Dynamic friction polishing (DFP) was proposed in the aim of improving the polishing efficiency of diamond, which utilizes the heat produced by high-speed friction between the metal polishing plate and the diamond substrate to convert diamond carbon into non-diamond carbon [18–20]. Subsequently, the non-diamond carbon is either removed by the mechanical shear of rotating metal plate, oxidization to form CO or CO_2, or diffusion into metal plate. However, high polishing load and fast sliding speed in DFP induce cracks and damage on the diamond surface [21,22]. Laser is another promising technique to polish diamond for its high energy intensity, high precision, high efficiency, and non-contact characteristics. Liu et al. adopted a 355 nm nanosecond laser to polish diamond in ambient air and obtained a surface with *Ra* roughness of 8.02 nm in the area of 20 × 20 μm^2 by AFM, and the diamond after polishing showed a high transmittance up to 80 % of the mechanically polished diamond in the visible spectrum [23]. Although laser polishing is highly efficient and capable of polishing complex shape and micro-structures of diamond, it is difficult to obtain a surface with relatively low roughness since it is rather challenging to precisely control the graphitization transition on the diamond surface [23,24].

Plasma etching has been widely used in semiconductor manufacturing for lithography etching, damage removal, and surface cleaning for its good repeatability, high efficiency, and strong versatility, presenting great potential in smoothing of difficult-to-machine semiconductor materials [25–29]. Ri et al. etched diamond (001) surface with hydrogen plasma and found that an atomically flat surface can be obtained if misorientation angle is larger than 1.5° due to the anisotropic etching of diamond for which the step edges are active sites [30]. Kuroshima et al. found that the trench structure of the diamond (111) evolved from square-shaped to triangular-shaped after hydrogen plasma etching for 100 h and suggested the different etching rate for carbon atoms based on their bonding state, indicating the anisotropic etching of diamond [31]. Furthermore, Xie et al. controlled the etching conditions of oxygen plasma to achieve anisotropic etching along muitiple crystal directions in diamond and applied this technique to fabricate monolithic diamond nanopillars [32]. These studies demonstrate the anisotrophic etching of diamond through different plasma sources, with the principle of anisotropy attributed to varying etching rate for different etching sites, carbon atoms with different bonding states, and different crystal planes. Recently, plasma-based atom-selective etching (PASE) was proposed to smooth single crystal silicon based on the mechanism that fluorine atoms with high oxidation potential in fluorine-containing plasma would selectively etch Si atoms with less activation energy [25]. Similar to the anisotrophic plasma etching mentioned above, PASE would also selectively etch diamond surface carbon atoms. However, PASE is based on the principle that carbon atoms with more dangling bonds would be preferentially removed and the removal rate is extremely high, and an atomic-scale smooth surface with the same bonding state would form finally. Herein, oxygen plasma under atmosphere was first adopted to successfully achieve PASE of SCD, obtaining an atomic-scale smooth surface with extremely high smoothing efficiency. The smoothing mechanism was verified by demonstrating the relationship between MRR and the experiment parameters (flow rate of oxygen, radio frequency (RF) power, and torch-wafer distance). To reveal the specific smoothing process, the *Sa* roughness and MRR evolution were conducted. Further X-ray photoelectron spectroscopy (XPS), Raman spectroscopy, and transmission electron microscopy (TEM) analyses verify the ability of PASE to remove subsurface damage without introducing extrinsic components during the smoothing of SCD process, proving the formation of an atomic-scale smooth surface for SCD. Oxygen plasma was also confirmed to effectively smooth SCD regardless of the initial surface conditions, sizes, and the crystal planes, showing the powerful applicability of PASE for SCD with various initial conditions.

2. Experiment details

2.1. Materials and characterization methods

SCDs (100) with 4 × 4 × 2 mm^3 dimensions, SCDs (110) and (111) with 3 × 3 × 1 mm^3 dimensions, and SCDs (100) with 8 × 8 × 0.5 mm^3 dimensions were used in the experiment. Here, all SCD raw materials were purchased from Xi'an Jingmeida Electronic Information

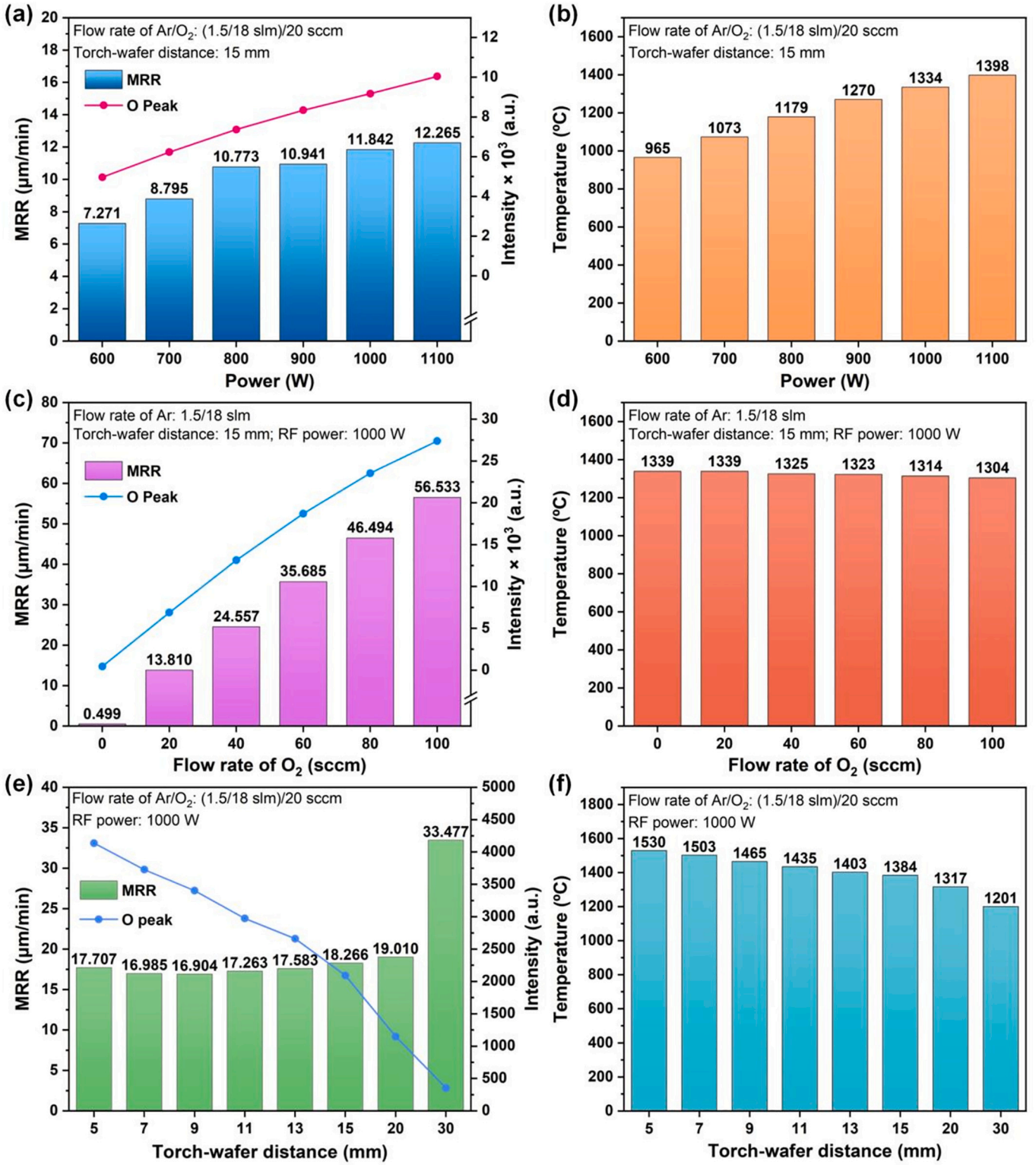

Fig. 4. The effect of RF power on (a) MRR, the concentration of oxygen radicals and (b) SCD surface temperature. The effect of oxygen flow rate on (c) MRR, the concentration of oxygen radicals and (d) SCD surface temperature. The effect of torch-wafer distance on (e) MRR, the concentration of oxygen radicals and (f) SCD surface temperature.

Technology Co., LTD (China) and the roughness of them were all about 2 nm (AFM, 20 × 20 μm^2). Non-selective oxygen plasma etching and coarse grinding were used to roughen (100) SCDs, increasing the roughness to around 60 nm and 450 nm (AFM, 20 × 20 μm^2). Further precisely mechanical polishing was also conducted to obtain a smoother initial surface of SCD (100) with the roughness of about 1.3 nm (AFM, 20 × 20 μm^2). SCDs with (110) and (111) crystal planes were also etched by oxygen plasma, creating rough initial surfaces with the roughness of 111 nm and 37.5 nm (AFM, 20 × 20 μm^2), separately.

Inductively coupled plasma (ICP) was characterized by optical emission spectroscopy (OES, Ocean Optics USB2000 + UV-VIS-ES) to detect the active species in the plasma. The temperature of SCD surface

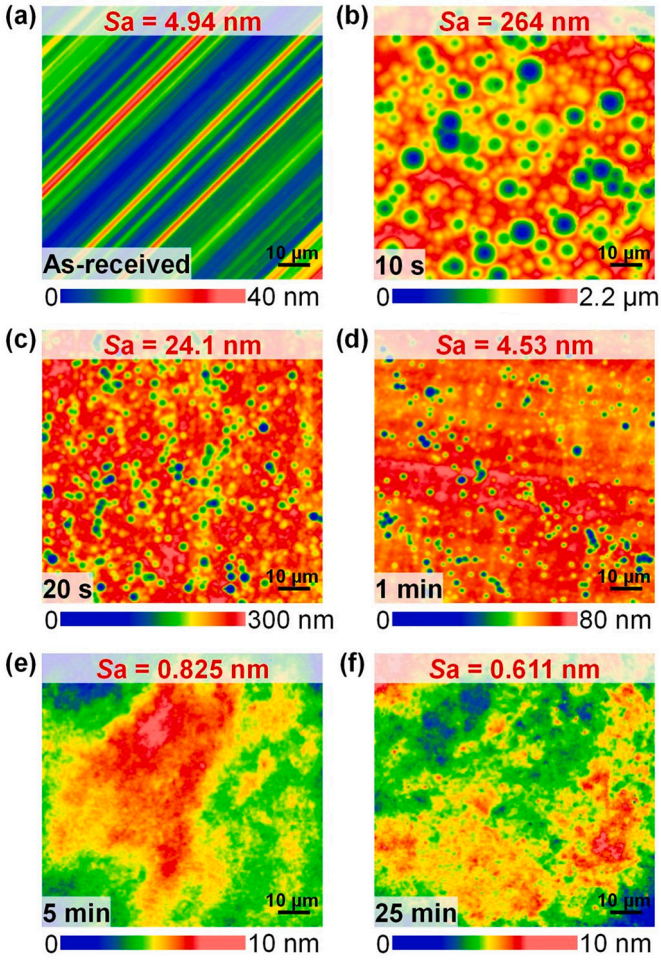

Fig. 5. Morphological changes at large scale during the smoothing process. (a)–(f) 3D optical surface profiler images for the as-received SCD and SCDs under 10 s, 20 s, 1 min, 5 min, and 25 min smoothing duration, respectively.

during oxygen plasma treatment was measured by an infraction imager (FLIR T660). AFM (Bruker Dimension Edge), scanning white light interferometry (SWLI, TAYLOR HOBSON CCI), and 3D optical surface profiler (NewView™ 9000, Zygo) were used to analyze SCD surface morphology and measure the roughness. Laser scanning confocal microscopy (LSCM, KEYENCE VK-X1000) was used to observe the surface morphology.

The weight of SCD samples before and after smoothing were measured by a precision balance (XSR105, METTLER TOLEDO) with a readability of 0.01 mg. The MRR can be evaluated by the following equation:

$$\mathrm{MRR} = \frac{10^3 \times \Delta m}{\rho \times S \times t}$$

where Δm (g) is the mass loss of SCD during the reaction process, ρ (3.5 g/cm^3) is the density of SCD, S represents the surface area of SCD (cm^2), t (min) is the total reaction time, and MRR (μm/min) is the removal rate of SCD.

The chemical composition of SCD surface before and after oxygen plasma smoothing was examined by X-ray photoelectron spectroscopy (XPS, ULVAC-PHI) which equipped with a PHI 5000 Versaprobe III spectrometer and Al $K\alpha$ X-ray radiation (1486.6 eV) source. All peaks have been calibrated by C 1s (284.8 eV) corresponding to the carbon contamination. Raman spectroscopy (HORIBA LabRAM HR Evolution) with a 785 nm laser source was utilized to compare the characteristic peaks changes and analyze the removal of non-diamond carbon on SCD surface during oxygen plasma smoothing process. To investigate the removal of surface defects and subsurface damage of SCDs, and to verify the formation of atomic-scale smooth surface, transmission electron microscopy (TEM, FEI Titan Themis G2 TEM ThermoFisher) was utilized. All TEM samples were fabricated based on a focused ion beam (FIB, Helios 450 s ThermoFisher) system. It is worth mentioning that to avoid the possible damage caused during the FIB process, a protective carbon layer was first applied to all SCD substrates. The energy dispersive spectroscopy (EDS, Super-X ThermoFisher) results were obtained through semi-quantitative measuring the elements' distribution in the cross sections part.

2.2. Smoothing mechanism and experimental setup of ICP

The smoothing of SCD is based on the mechanism of PASE which is shown in Fig. 1. Normally, carbon atoms in diamond would bond with another four carbon atoms and form stable carbon-carbon covalent bonds with strong bond energy. However, defects and subsurface damage on SCD surface caused by applying hard abrasives and high pressure load during mechanical polishing process would lead to inhomogeneous bonding state of diamond and deteriorate diamond surface quality. During the smoothing of SCD, carbon atoms under the radiation of oxygen plasma would obtain sufficient excitation energy and are absorbed by reactive oxygen atoms, and then C—C bonds would tend to break to form CO/CO_2. For those carbon atoms with three dangling bonds, only one C—C bond requires to be broken to form carbon oxides molecules. As a consequence, the active oxygen radicals would tend to react with carbon atoms with three dangling bonds first. Once a CO/CO_2 molecule forms, it would dissociate from the wafer surface, and a carbon atom is removed. Owing to different number of dangling bonds of different carbon atoms on the surface of SCD, the removal priority of carbon atoms varies and it can be defined as V_1, V_2, V_3, and V_4 according to the number of C—C bonds. In the process of PASE, there would be $V_1 > V_2 > V_3 > V_4$ and carbon atoms with only one C—C bond would be preferentially removed. Once carbon atoms with higher etching preference are removed, the lower layer of carbon atoms would be exposed, and the surface bonding state is continuously changing. As PASE process goes on, the surface of SCD would experience several steps to remove carbon atoms with different priorities to eliminate the non-equilibrium state. In the end, all carbon atoms on the surface of SCD possess the same bonding state and an atom-level equilibrium smooth surface forms. As is described in Fig. 1, the initial surface of SCD is in a non-equilibrium state with carbon atoms carrying different number of dangling bonds. Among these carbon atoms, two atoms marked with red dotted line possess the highest removal priority and would be removed in step 1. Then, carbon atoms under the removed atoms are exposed and the surface state changes to the second state. In this state, there are no carbon atoms with three dangling bonds on the surface and carbon atoms with two dangling bonds would be removed in step 2. Additionally, the lower layer of carbon atoms is exposed after step 2 and the bonding state of carbon atoms on the surface is still in the non-equilibrium state. Thus, carbon atoms with higher removal priority are removed through step 3. However, the surface state of SCD remains non-equilibrium after step 3, and another removal process continues, namely step 4. Thereafter, carbon atoms on the surface of SCD are in the equilibrium state and the surface becomes atomic-scale smooth.

ICP setup mainly consists of five parts, namely power supply part (automatic radio frequency (RF) match controller and RF power), plasma ignition part (torch clamp, inductance coil, electric spark generator, and quartz tubes), gas supply part (Ar cylinder, O_2 cylinder, gas delivery lines, and mass flow controllers (MFC)), numeric controller (NC) machine part (3-axis NC platform and sample holder) and water cooling part. Among them, plasma ignition part is the most important component which is used to generate reactive plasma. ICP quartz tubes consist of coaxial outer and inner tubes. In the experiment process, oxygen and argon are transported through gas delivery lines to inner

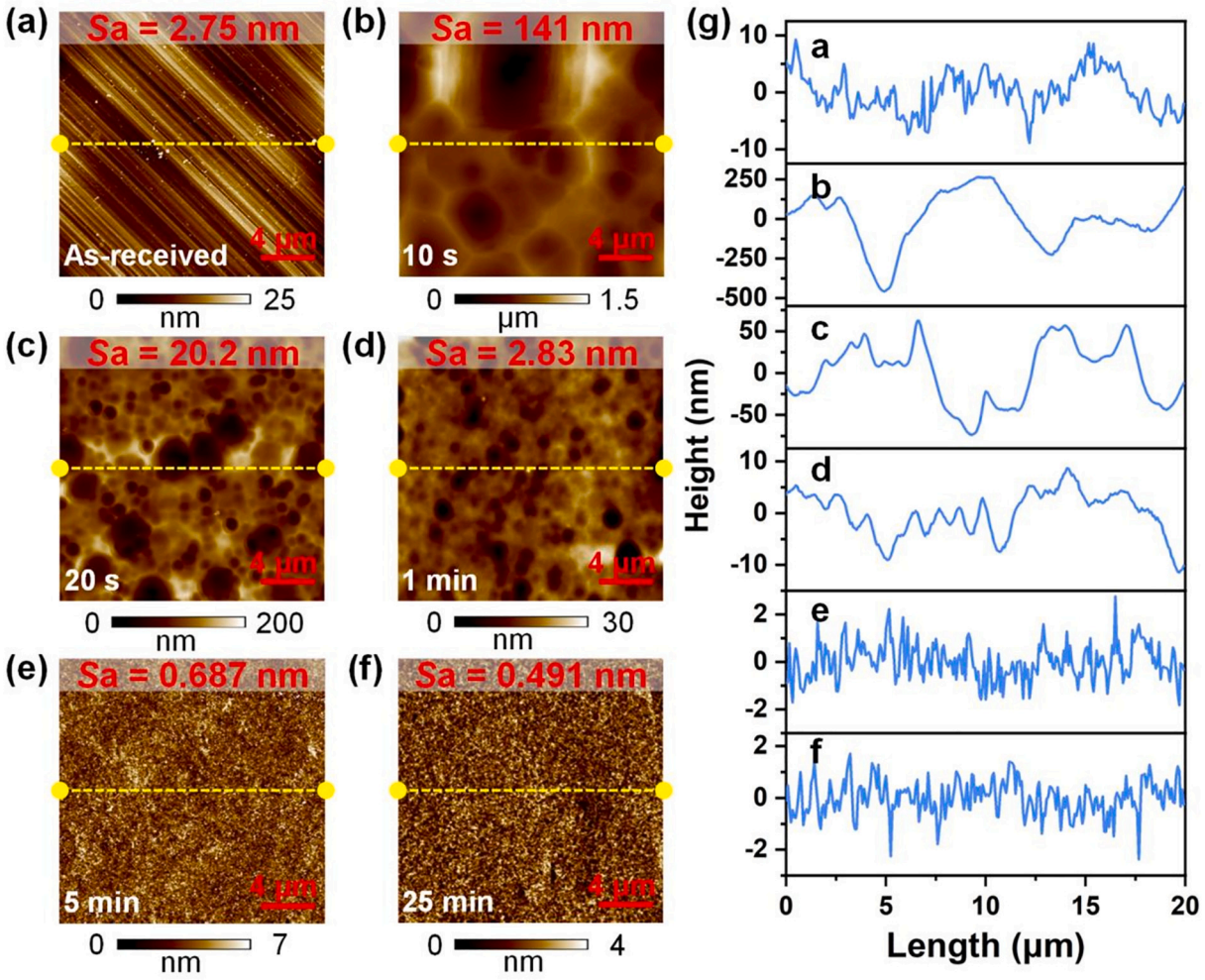

Fig. 6. Morphological changes at small scale during the smoothing process. (a)–(f) AFM images for the as-received SCD and smoothing of SCDs under 10 s, 20 s, 1 min, 5 min, and 25 min, respectively. (g) Corresponding section profiles of (a)–(f).

quartz tube. Argon also conducts as cooling gas which is injected tangentially into the gap between the outer tube and the inner tube. Once high voltage spark generator is ignited, argon in the inner tube would be ionized and form stable plasma under the action of the magnetic field generated by inductance coil. Then, oxygen would also be supplied into the inner tube and ionized under the collision bombardment caused by Ar^+ and electrons, generating oxygen plasma.

2.3. Schemes of experiment

Since carbon atoms have the tendency to react with oxygen atoms under sufficient energy and form CO_2 or CO gases, it's reasonable to infer that oxygen plasma would have the ability to react with diamond which is composed entirely of carbon atoms. In this study, a series of comprehensive experiments were conducted to investigate the impact of different smoothing parameters on the specific process of smoothing, as well as changes in surface morphology and roughness during a 25 min smoothing process. Additionally, the alterations in surface composition and subsurface damage of SCD were examined, along with exploring the applicability of PASE under various initial conditions.

First, the smoothing process was investigated. A comparison between pure argon plasma and oxygen plasma was conducted to verify the existence of oxygen active radicals. RF power, flow rate of oxygen, and torch-wafer distance were set as 1000 W, 20 sccm, and 15 mm, separately. To find appropriate technical parameters to smooth SCD, a group of orthogonal experiments were attempted with three factors (flow rate of oxygen, RF power, and torch-wafer distance) and three levels for each factor. Factor 1 has levels of 20 sccm, 60 sccm, and 100 sccm; factor 2 has levels of 600 W, 800 W, and 1000 W; and factor 3 has levels of 5 mm, 10 mm, and 15 mm. Nine different combinations of three factors are randomly generated to ensure the objectivity of the experiment. The specific experiment design is shown in Table 1 and all SCDs used in this experiment were etched by oxygen plasma at 600 W RF power and the *Sa* roughness was about 100 nm after the etching treatment. The phenomena of orthogonal experiments were further explored to find the relation between each factor and MRR of SCD and experiment parameters are shown in Table 2(a). In this part, all SCDs were (100) crystal plane with $4 \times 4 \times 2$ mm^3 dimensions.

Secondly, surface morphology and roughness evolution characterized by AFM and 3D optical surface profiler were investigated to demonstrate the surface morphology and the minimum roughness of SCD (100) during the long-term smoothing process. All experiments in this part were conducted under the same parameters, shown in Table 2 (b).

Thirdly, SCDs (100) were coarse ground with 750 N load by using a mechanical polishing device for 10 min first. Then, one of SCDs was smoothed by oxygen plasma for 15 min at the parameters shown in Table 2(b). The final surface composition and subsurface damage of SCD (100) before and after smoothing was characterized by XPS, Raman spectroscopy, TEM, and EDS.

Finally, SCDs (100) with different initial surface conditions were fabricated through coarse grinding, oxygen plasma etching at 600 W RF

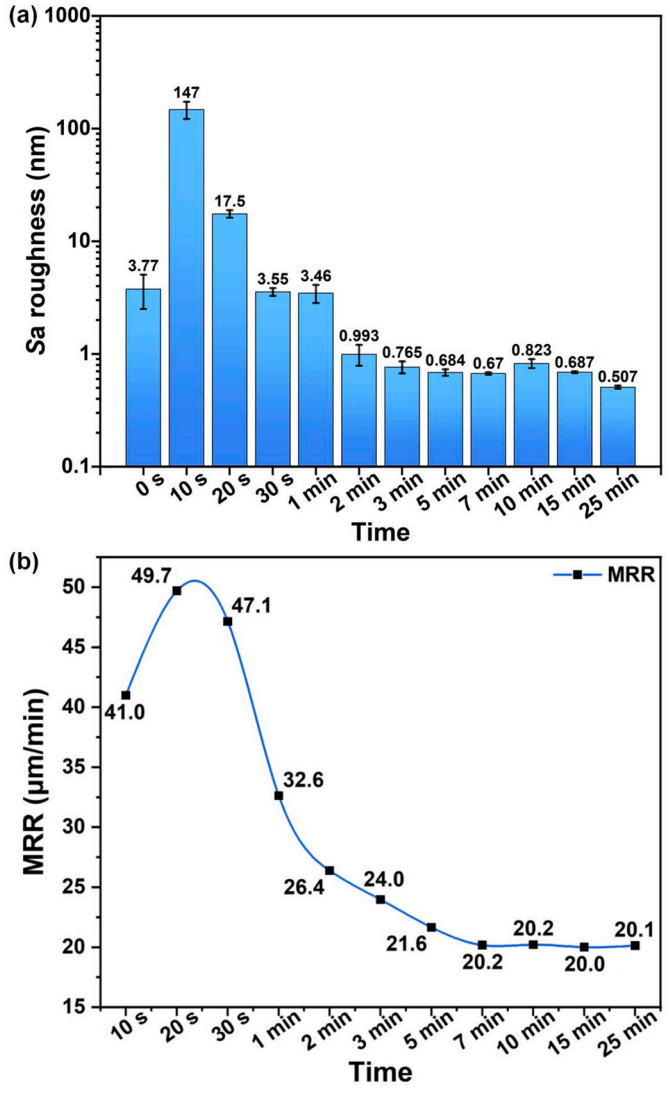

Fig. 7. Surface roughness and MRR evolution. Evolution of (a) Sa roughness and (b) MRR during 25 min smoothing process of SCD.

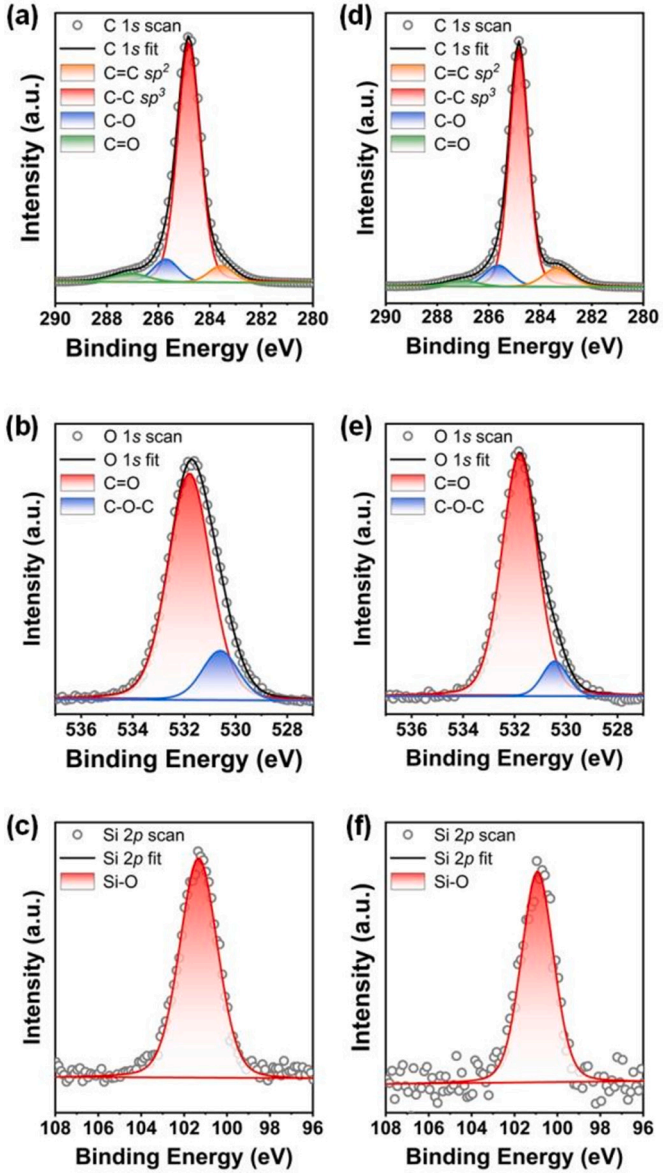

Fig. 8. XPS of SCD surface. (a) C 1*s*, (b) O 1*s*, and (c) Si 2*p* of as-received SCD. (d) C 1*s*, (e) O 1*s*, and (f) Si 2*p* of SCD after smoothing.

power, and precisely mechanical polishing. As-received SCD (100) as well as other three SCDs with different initial surfaces were smoothed by oxygen plasma for 15 min. The surface before and after smoothing were compared to investigate the smoothing dependence of PASE on the initial surface conditions of SCD. Larger piece of SCD (100) with 8 × 8 × 0.5 mm^3 dimensions was adopted to verify the ability of PASE to smooth a large size of SCD. Before smoothing, the diamond was etched by oxygen plasma at 600 W RF power, and then smoothed by oxygen plasma at 1000 W RF power for 15 min. SCDs (110) and (111) with 3 × 3 × 1 mm^3 dimensions were used to verify the independence of PASE on crystal planes of SCD. These SCDs were etched by oxygen plasma at 600 W first and then smoothed by oxygen plasma at 1000 W RF power for 5 min. The surfaces before and after smoothing were measured to demonstrate the smoothing results.

Since SCDs are likely to react with ambient oxygen under high temperature, a torch-down step was adopted to lower the influence of ambient oxygen. Specifically, after oxygen plasma treatment, RF power was first shut down and then the supply of oxygen was stopped. Immediately afterwards, torch-wafer distance was reduced to fully enclose SCD, and argon was supplied for 2 min to cool down SCD and shield the sample from ambient oxygen [29].

3. Results and discussion

3.1. Exploration of the smoothing process

To verify the existence of reactive radicals, OES was conducted on pure argon plasma and oxygen plasma. As is shown in Fig. 2(a) and (b), both oxygen and pure argon plasma exhibit light purple color outer flame, bright white inner flame, and flame core, and little difference between oxygen plasma and pure argon plasma could be found through visual observation of plasma torch. OES characterization in Fig. 2(c) clearly demonstrates that argon emission line dominates the wavelength from 700 to 850 nm for these two kinds of plasma. Ar^-/N_2^+, O_2^+, and O^+ characteristic peaks spread in the range of 400 to 700 nm, which are both detected in oxygen and pure argon plasma. These emission peaks are attributed to argon, ambient oxygen, and nitrogen. However, an obvious peak at 777.3 nm can be found only in oxygen plasma, which corresponds to the peak of oxygen radicals [33]. This result reveals that the addition of oxygen would contribute to the generation of oxygen radicals which would be highly reactive with carbon atoms.

Since the concentration of reactive species and energy input

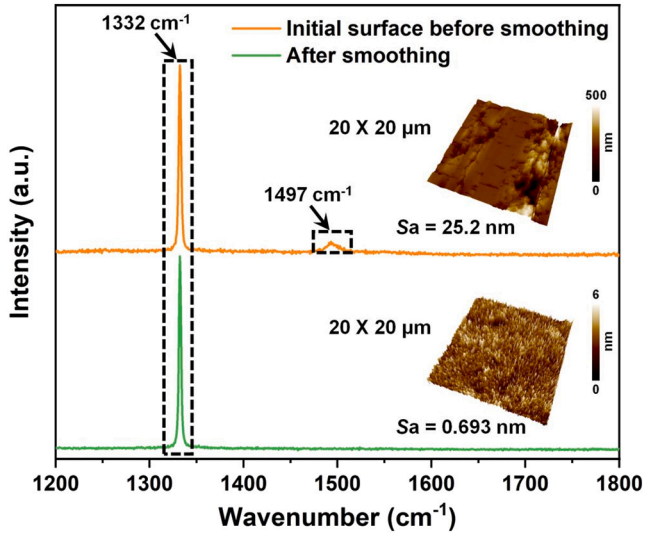

Fig. 9. Raman spectra of SCD before and after smoothing.

determine the reaction process and the final surface quality, three different ingredients: flow rate of oxygen, RF power, and torch-wafer distance were chosen as three factors to conduct orthogonal experiments. As is shown in Table 1, the worst result could be obtained when the experiment was conducted under 60 sccm oxygen flow, 600 W RF power, and 15 mm torch-wafer distance. The final 105 nm *Sa* roughness of SCD indicates that there was no smoothing effect under this experiment condition. However, the best smoothing result with 0.302 nm *Sa* roughness could be achieved when RF power and torch-wafer distance change to 1000 W and 5 mm, respectively. These two different results could be ascribed to the lower energy input under the condition of lower RF power and larger torch-wafer distance. Further analysis of the *Sa* roughness for each of combinations revealed the estimates of level effects for each factor, corresponding to I, II, and III in Table 3. Specifically, for factor 1, I represent the estimate of 20 sccm, II represent the estimate of 60 sccm, and III represent the estimate of 100 sccm. Similarly, for factor 2, I represent the estimate of 600 W, II represent the estimate of 800 W, and III represent the estimate of 1000 W. Additionally, for factor 3, I represent the estimate of 5 mm, II represent the estimate of 10 mm, and III represent the estimate of 15 mm. The value of the estimate of level effect is obtained by the *Sa* roughness sum of the corresponding level. For example, estimate of 600 W is the *Sa* roughness sum of number 1, 4 and 7 since 600 W is one of the chosen factor for these three combinations. By choosing the smallest estimates of different levels, the smoothing experiment reference parameters thus can be evaluated to be 20 sccm oxygen flow rate for factor 1, 1000 W RF power for factor 2, and 5 mm torch-wafer distance for factor 3. However, too short torch-wafer distance would contribute to much heat accumulation and cause the crack of sample holder. To avoid inconsistencies in experimental conditions due to the replacement of cracked sample holder, 15 mm torch-wafer distance was decided to be the final smoothing experiment parameter.

To elucidate the significant surface difference when adopting different energy input, SCDs (100) with even mechanical scratches, defined to be as-received samples, were treated with oxygen plasma at 600 W RF power and 1000 W RF power for 25 min, respectively. Fig. 3 (a) and (d) shows the initial surface morphology of SCD and there were many mechanical scratches spreading all over the surface both in AFM and SWLI measurement areas. After oxygen plasma treatment at 600 W for 25 min, a large number of point-bottom etch pits appeared on SCD (100) surface, shown in Fig. 3(b) and (e). These point-bottom etch pits were related to the presence of “intrinsic” dislocations in the crystal [34]. Their appearance deteriorated the surface quality and increased the *Sa* roughness from 2.25 and 5.65 nm to 114 nm and 5.62 μm, corresponding to the no smoothing result listed in Table 1. In contrast to the deterioration of surface quality at 600 W RF power, the surface of SCD (100) could be smoothed effectively at 1000 W RF power and the *Sa* roughness could be reduced to 0.632 and 0.766 nm, as depicted in Fig. 3 (c) and (f).

An infraction imager was utilized to measure the average temperature of SCD surface under the radiation of plasma. As is shown in Fig. 3 (g), all infraction images are adjusted to the same temperature range from 100 to 1500 °C and the center of SCD at 1000 W is much brighter than at 600 W. The average temperature of SCD surface at 1000 W reaches up to 1338.9 °C compared with 965.4 °C at 600 W. Based on the results above, it can be concluded that RF power would determine the temperature of SCD surface and oxygen plasma torch, namely the energy input of the reaction system. When oxygen plasma is ignited at 600 W RF power, both the concentration and energy of oxygen active radicals are far from the prerequisites for PASE of SCD, which is completely different from that at 1000 W RF power.

During the process of oxygen plasma treatment, both the reaction rate and the smoothing results depend on the concentration of reactive species and energy of the system. Fig. 4 specifically describes the effect of RF power, flow rate of O_2, and torch-wafer distance on MRR, the intensity of O peak, and the surface temperature of SCD (100). According to the results shown in Fig. 4(a), the intensity of O peak increases almost linearly along with the increase of RF power, which contributes to the rise of MRR. Combined with the results shown in Fig. 4 (b), it can be concluded that the increase of RF power raises the surface temperature of SCD and simultaneously generate a higher concentration of highly reactive oxygen radicals, resulting in a faster reaction rate. It is worth noting that in the experiment of RF power change, the surface morphology and roughness of the SCDs after treatment were also characterized, which are shown in Fig. S1 and S2. When RF power is at 600 W, the concentration of reactive species and energy of the system are not sufficient, and the plasma treatment would generate the etching mode, creating the etch pits morphology of SCD. However, the smoothing mode would appear when RF power reaches 900 W, and the *Sa* roughness of the smoothed surface is in the subnanometer range, indicating the effect of atom-selective etching caused by temperature modulation. Fig. 4(c) and (d) shows the increase of the intensity of O peak and MRR are consistent with the increase of flow rate of O_2 while the corresponding temperature decreases slightly. Therefore, flow rate of O_2 plays a key role in adjusting the intensity of O peak and MRR when RF power remains constant at 1000 W. This result reveals the dependence of MRR on the concentration of reactive oxygen radicals.

The relationship among torch-wafer distance, the intensity of O peak, and MRR is demonstrated in Fig. 4(e) and (f). As torch-wafer distance increase at every 2 mm pitch, the temperature of SCD surface drops down step by step and the intensity of O peak decreases in the meantime. However, the change of MRR is not corresponding to the decrease of the intensity of O peak. MRR experiences a slight decrease from 5 mm to 9 mm torch-wafer distance at the beginning. Then it gradually increases from 17.263 μm/min at 11 mm to 33.477 μm/min at 30 mm. This paradox could be attributed to the introduction of ambient oxygen which would react quickly with SCD under high temperature in a short time. In this experiment, SCD after plasma treatment were in high temperature state with a deep orange color surface. In torch-down step, 3-axis NC platform moved up quickly until SCD was fully enclosed by quartz tubes to shield the wafer from reacting with ambient oxygen. In the beginning, the increase of torch-wafer distance would reduce the energy input and the concentration of reactive oxygen radicals on the surface of SCD, thus resulting in a decreasing MRR. As the torch-wafer distance continued to increase, the time spent in torch-down step would increase, which inevitably resulted in longer contact time between ambient oxygen and SCD, causing undesired etching reaction. When torch-wafer distance began to increase, the increase of time in torch-down step was insufficient to cause a significant impact on MRR,

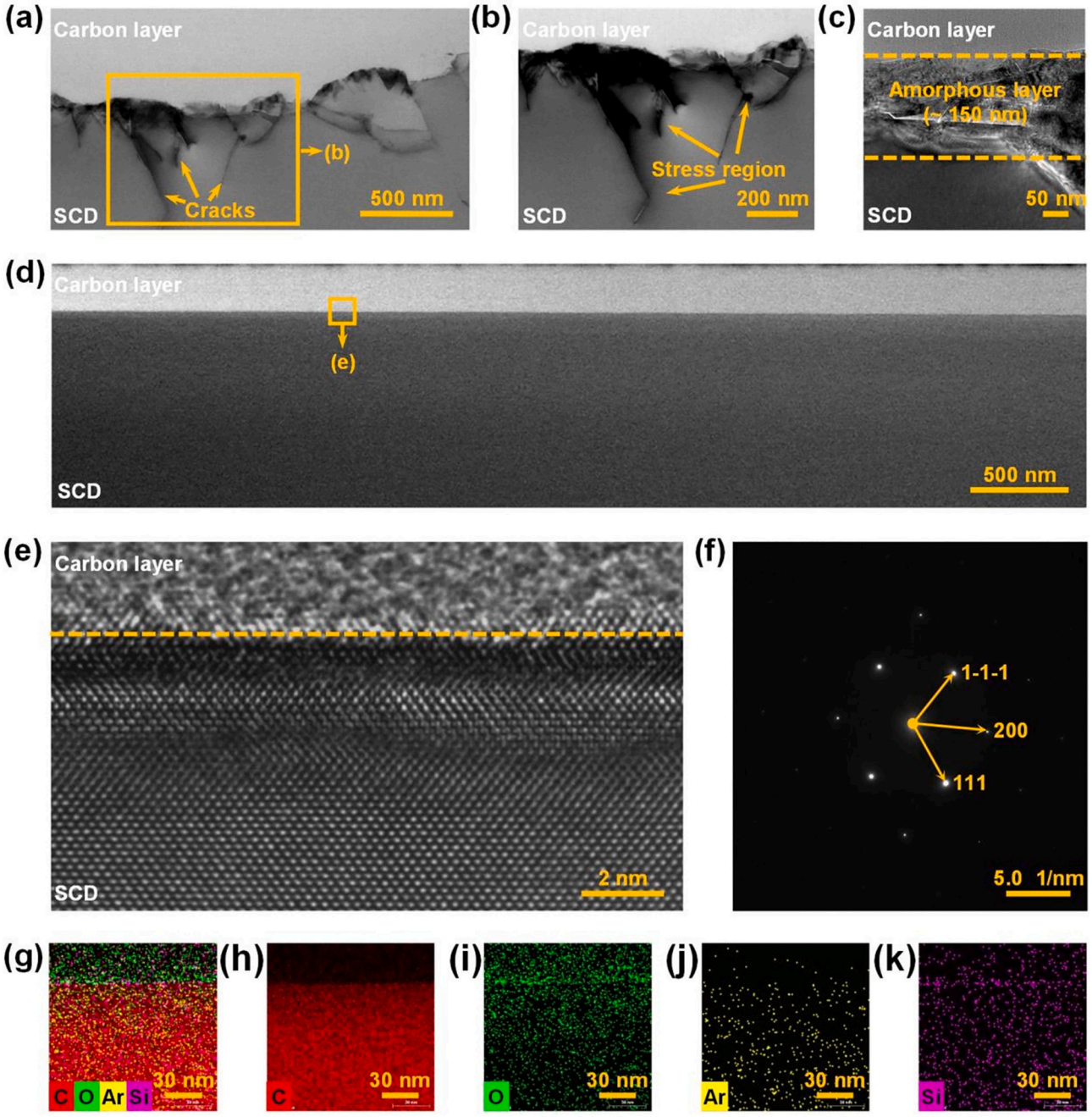

Fig. 10. TEM results of SCD (100) substrates before and after smoothing. (a)–(c) TEM images for the initial surface before smoothing. (d–e) TEM images of SCD (100) substrate after smoothing. (f) Selective area electron diffraction pattern obtained on SCD (100) substrate after smoothing. (g)–(k) EDS mapping results of SCD (100) substrate after smoothing. (g) Elements overlap image. (h)–(k) Elemental maps of C, O, Ar, and Si, respectively.

and the decrease of temperature and concentration of oxygen radicals determined the decrease of MRR. However, when torch-wafer distance came to 11 mm, the reaction between SCD and ambient oxygen could not be neglected, resulting in the increase of MRR. The reaction would even become the main reason for the removal of SCD when torch-wafer distance reached 30 mm, and the surface of SCD after oxygen plasma treatment was in a blurry opaque state because of the existence of etch pits. These etch pits were generated due to the etching reaction between ambient oxygen and SCD. To avoid the deterioration of surface quality of SCD after oxygen plasma smoothing, a proper torch-wafer distance and a quick torch-down step are necessary.

3.2. Surface morphology evolution

SCD (100) can be smoothed from hundred nanometer roughness to subnanometer roughness through oxygen plasma smoothing. Here, the surface morphology evolution of PASE of SCD (100) were explored and the adopted SCD samples were all as-received with about 2 nm *Sa* roughness. The experiment parameters refer to Table 2(b). Fig. 5 demonstrates the morphological changes of SCD at large scale measured by 3D optical surface profiler. Obvious morphological difference can be observed from Fig. 5(a) and (b). After 10 s oxygen plasma treatment, the as-received surface became uneven and there were many point-bottom etch pits spreading all over it, with *Sa* roughness increasing from 4.94 to 264 nm. With the continuation of PASE, large etch pits were removed

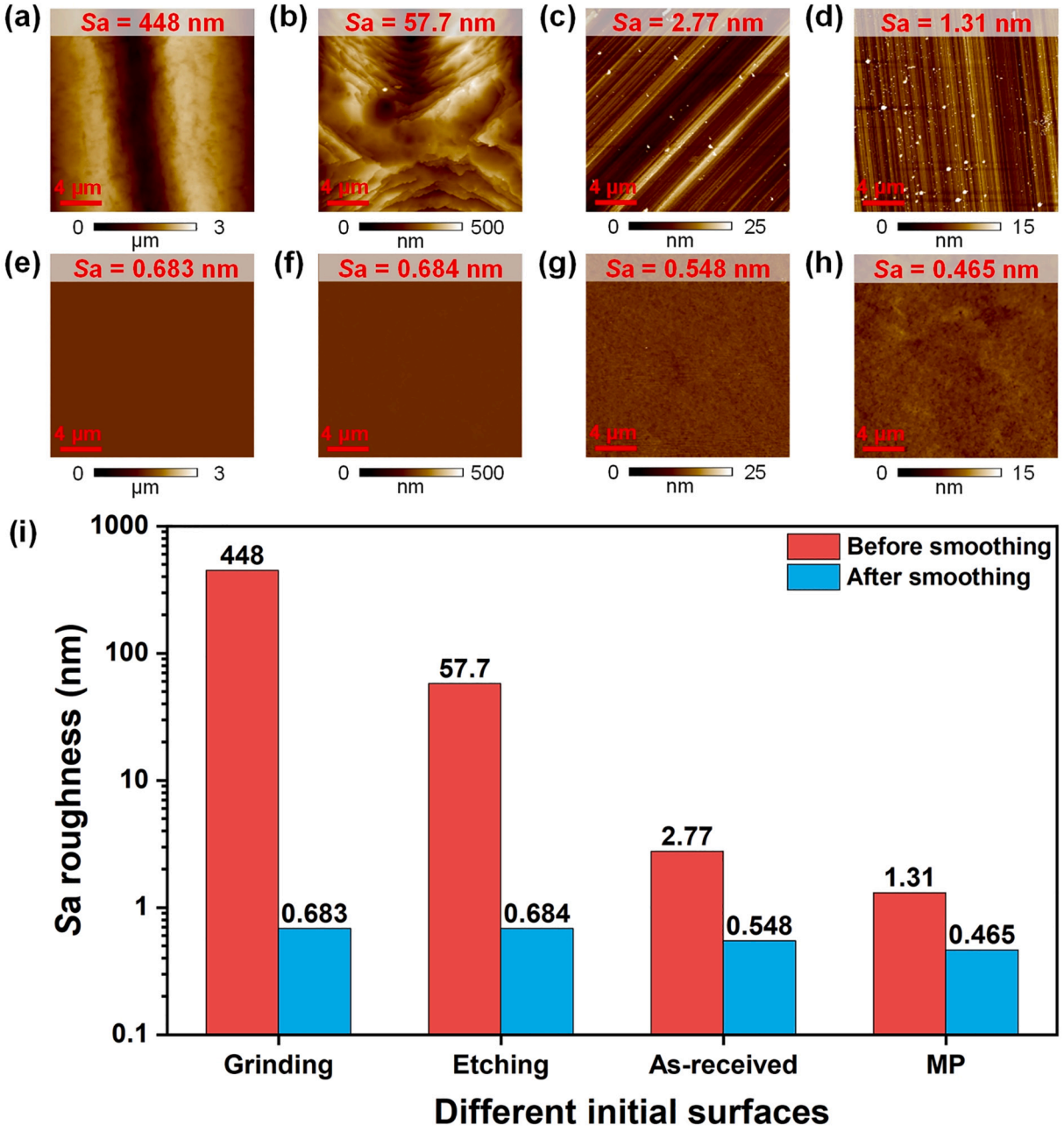

Fig. 11. PASE smoothing of SCDs with different initial surfaces at 1000 W RF power for 15 min. (a–d) SCDs with coarse grinding, oxygen plasma etching at 600 W RF power, as-received, and precisely mechanical polishing initial surface. (e–h) SCDs after smoothing. (i) *Sa* roughness comparison before and after smoothing of SCDs with different initial surface.

from SCD surface and lots of small etch pits appeared on the surface of SCD, which can be seen from Fig. 5(c). Due to the disappearance of large etch pits, the roughness experienced a quick drop from 264 nm to 24.1 nm in only 10 s. Fig. 5(d)–(f) indicate that further smoothing would contribute to the disappearance of small etch pits and the formation of an ultra-smooth surface. The *Sa* roughness of SCD surface could finally decreased to 0.611 nm in the area of 87.5 × 87.5 μm^2.

During the initial stage of SCD smoothing, oxygen plasma torch was just ignited and failed to generate sufficient highly reactive oxygen radicals due to the lack of energy accumulation in the beginning. Meanwhile, the temperature of SCD surface was far from reaching the temperature threshold for PASE of SCD. Lack of enough oxygen radicals with highly reactive activity and the relative low surface temperature of SCD resulted in oxygen plasma non-selective etching at the beginning of smoothing of SCD. The etch pits that spread all over SCD surface were in sharp bottom, similar to the result shown in Fig. 3(e). With the extension of smoothing process, the temperature of oxygen plasma stabilized at around 1330 °C, and the etching behavior transferred to PASE behavior, removing the etch pits and forming an ultra-smooth surface.

Fig. 6(a)–(f) reveals the surface morphology evolution of SCD at small scale using AFM. The measurement area is 20 × 20 μm^2 and the morphology evolution tendency of SCD is consistent with that at large scale. The *Sa* roughness of SCD can be reduced from 2.75 nm to 0.491 nm through 25 min smoothing. Fig. 6(g) is the corresponding section profile at different smoothing duration shown in Fig. 6(a)–(f). The profiles shown in Fig. 6(g) demonstrate that the section height fluctuates within 20 nm in the length of 20 μm before smoothing. After 10 s smoothing, etch pits with several micrometers diameter dominated the

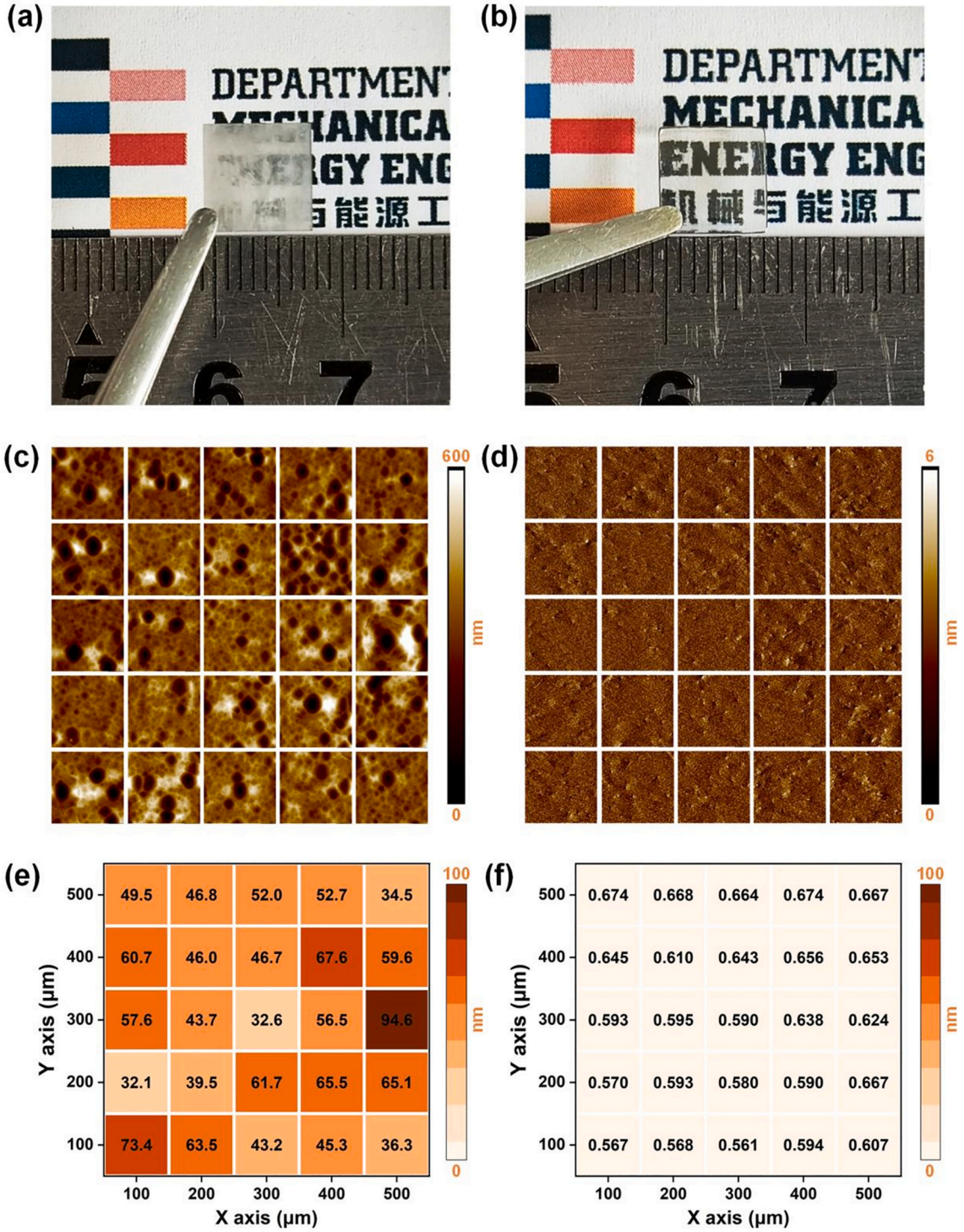

Fig. 12. PASE smoothing results of SCD (100) with dimensions of 8 × 8 × 0.5 mm^3. Optical images of SCD (100) (a) before and (b) after smoothing. (c) Surface morphology of SCD (100) before smoothing and (e) the corresponding *Sa* roughness distribution. (d) Surface morphology of SCD (100) after smoothing and (f) the corresponding *Sa* roughness distribution.

surface of SCD and the fluctuation of section height widened to 750 nm. Only 10 s later, the fluctuation decreased to 150 nm, indicating the disappearance of deep etch pits. Though there were still many small etch pits on SCD surface after smoothing for 1 min, the fluctuation of section profile had recovered to the initial fluctuation range. After smoothing of SCD for 5 min, the height fluctuated within 5 nm and the corresponding surface was in an ultra-smooth state. By increasing the smoothing time to 25 min, the surface fluctuations did not show any further reduction, suggesting that the diamond surface had reached its smoothing limit.

Sa roughness evolution over 25 min smoothing is shown in Fig. 7(a). Five areas of each sample under different smoothing duration were measured by AFM to ensure the credibility of roughness results. The average *Sa* roughness of initial surface was 3.77 nm. After 10 s oxygen plasma etching, the average *Sa* roughness rose to 147 nm due to the formation of large quantity of etch pits. However, etching behavior transferred to PASE behavior quickly in the next 10 s and the average *Sa*

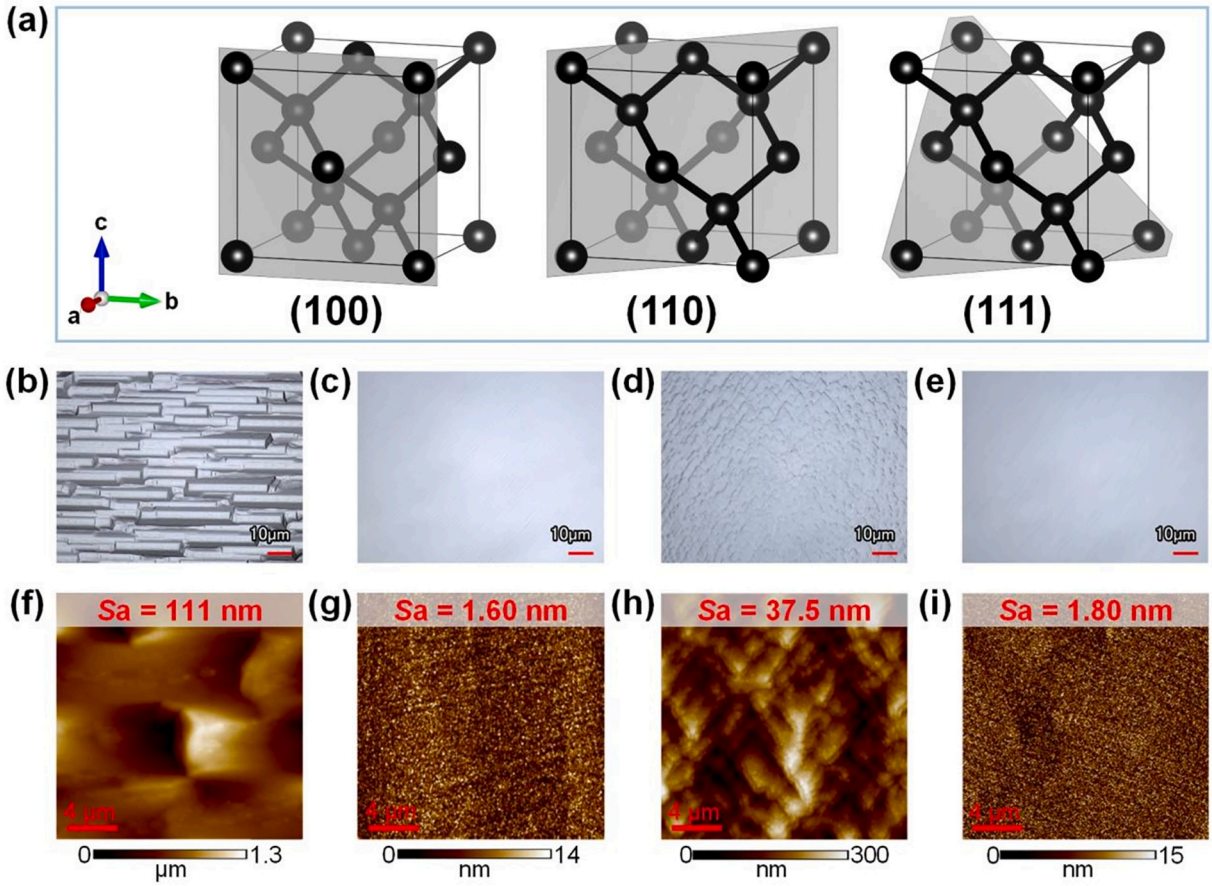

Fig. 13. PASE smoothing results of SCD with (110) and (111) crystal planes in dimensions of 3 × 3 × 1 mm^3. (a) Schematic diagram of SCD with (100), (110) and (111) crystal planes. (b–e) LSCM images of SCDs: surface of SCD (110) (b) before and (c) after smoothing, surface of SCD (111) (d) before and (e) after smoothing. (f–i) AFM images of SCDs: surface of SCD (110) (f) before and (g) after smoothing, surface of SCD (111) (h) before and (i) after smoothing.

roughness of SCD decreased to 17.5 nm. The average *Sa* roughness continued to decrease as PASE progressed and stabilized at around 0.5 nm after 5 min smoothing. Fig. 7(b) depicts MRR evolution during the smoothing process. MRR experienced a quick growth, then decreased gradually, and kept stable after 7 min smoothing. The highest MRR can reach 49.7 μm/min and the final MRR remained steady around 20 μm/min, which is still thousands of times higher than traditional MP and CMP of diamond, verifying the high efficiency of PASE for SCD [15,17]. The increase of MRR in the first 10 s can be attributed to two reasons. One is the expansion of the reaction area between oxygen plasma and SCD due to the formation of etch pits. Another reason is the exposure of defects of SCD after initial non-selective etching. The carbon atoms in the exposed defective sites tend to have more dangling bonds, resulting in a higher removal rate. After 20 s smoothing, the average *Sa* roughness decreased and there would be less reaction area and defects on SCD surface. Therefore, MRR began to decrease after first 20 s smoothing. After 5 min smoothing, all carbon atoms on the surface of SCD would reach a stable bonding state, thus resulting in a consistent MRR after 7 min smoothing.

3.3. Investigation on surface composition and subsurface damage

XPS and Raman spectroscopy in Fig. 8 shows the chemical bonding state of C, O, and Si on SCD surface before and after smoothing. Fig. 8 (a)–(c) demonstrate C 1*s*, O 1*s*, and Si 2*p* spectra of as-received SCD surface while Fig. 8(d)–(f) depict C 1*s*, O 1*s*, and Si 2*p* spectra of SCD after 15 min smoothing. Since saturated carbon (C—C) dominates in SCD and has the same binding energy (BE) position with contamination carbon (C—C), the peak of saturated carbon was directly used to calibrate all XPS data. As shown in Fig. 8(a), the C 1*s* spectra of as-received SCD can be fitted with four components according to BE: C—C sp^3 (BE: 284.8 eV), C═C sp^2 (BE: 283.6 eV), C—O (BE: 285.7 eV), and C═O (BE: 287.0 eV). C—C sp^3 peak dominates C 1*s* spectra, corresponding to diamond saturated carbon. C═C sp^2 peak located at 283.6 eV indicates the existence of non-diamond carbon on SCD surface layer. This characteristic peak may originate from the impurity contamination in SCD chemical vapor deposition (CVD) growth process [33]. Other miscellaneous peaks, namely, C—O and C═O, are probably coming from spontaneous oxidation under air or adsorption of carbon pollutant when contacting with air [35]. Fig. 8(b) describes the O 1*s* spectra of as-received SCD and there are two fitting BE peaks located at 530.6 eV and 531.8 eV. The one located at 530.6 eV corresponds to C-O-C and the dominant BE peak at 531.8 eV belongs to C═O. Si element was observed through XPS and the result is shown in Fig. 8(c). Deconvolution result reveals that only one Si—O peak located at 101.3 eV fits well with Si 2*p* spectra. The appearance of Si element can be attributed to the impurity introduced by the previous mechanical polishing since silicon is one of the composition of scaife polishing plate. There is rare difference of the chemical composition of SCD before and after smoothing. Only some insignificant changes happened in BE peak position of few chemical bonds. In Fig. 8(d), C═C sp^2 and C—O BE peak moved to 283.3 eV and 285.6 eV, respectively. Simultaneously, C—O—C of O 1*s* and Si—O of Si 2*p* in Fig. 8(e) and (f) decreased slightly to 530.4 eV and 100.9 eV, respectively.

Raman spectroscopy is a powerful optical characterization method to analyze the chemical composition, structure, configuration, strain, and crystallinity of different substance, especially the carbon materials [36]. Here, Raman spectroscopy was conducted to verify the impact of PASE

on the structure and chemical composition of SCD. As it can be seen from AFM images in Fig. 9, there are abundant mechanical scratches and subsurface damage on SCD (100) surface before smoothing, which were caused by the strong mechanical shear force during coarse grinding. After smoothing for 15 min, the surface of SCD (100) was smoothed and the *Sa* roughness was 0.693 nm. Raman spectrum from 1200 to 1800 cm^{-1} of SCD before smoothing consists of two characteristic peaks. The sharp spectrum peak locates at 1332 cm^{-1} is the intrinsic peak of diamond sp^3 hybridization. Another weak and broad peak at 1497 cm^{-1} represents the non-diamond sp^2-hybridised carbon on SCD surface caused by the strong mechanical action [37]. However, the mechanical scratches and non-diamond carbon were both removed after smoothing. The corresponding Raman spectrum shows that in the range from 1200 to 1800 cm^{-1}, only the intrinsic peak of diamond at 1332 cm^{-1} exists.

TEM and EDS were carried out to further analyze the evolution of surface defects, atomic structure, and the chemical composition of SCD. SCDs with many mechanical scratches and subsurface damage caused by coarse grinding were adopted as initial samples. One of SCDs was smoothed for 15 min and it became bright and transparent. The surfaces of SCD samples were both coated with a carbon protective layer to avoid surface damage introduced during the process of FIB thinning, and the protective layer existed at the uppermost gray layer in TEM images. Fig. 10(a)–(c) describes the surface of SCD before smoothing. It is clear that there are numerous cracks visible in the subsurface of SCD in Fig. 10 (a). Additionally, as depicted in Fig. 10(b), strong mechanical action caused local area deformation and formed stress region within the subsurface of SCD. Furthermore, Fig. 10(c) reveals the presence of an amorphous layer with a thickness of approximately 150 nm on the surface of SCD. These mechanical damage layers were completely removed through 15 min smoothing and the corresponding results can be seen in Fig. 10(d)–(e). As shown in Fig. 10(d), TEM image of SCD surface after 15 min smoothing presents a rather flat boundary between the upper carbon protective layer and the diamond substrate. A flat SCD substrate surface with well-arranged atoms can be observed in Fig. 10(e) and there were no structure defects detected on SCD subsurface, demonstrating the effectiveness of PASE in removing damage layer of SCD. The high crystal quality of SCD after PASE can also be verified by the clear single crystal pattern shown in Fig. 10(f). Additionally, the EDS mapping on the cross section of SCD surface after smoothing was conducted, which is shown in Fig. 10(g)–(k). Obviously, only carbon element can be detected on the cross section of SCD and this result demonstrates the fact that PASE would not introduce any other non-intrinsic elements into SCD during the smoothing process.

3.4. Verification of technology applicability

The above results and discussion have verified the smoothing ability of PASE on SCD (100) with the dimension of $4 \times 4 \times 2$ mm^3. Here, further experiments were designed to study the dependence of PASE on the initial surface conditions, the size of SCD, and crystal planes.

To construct different initial surface conditions of SCD, coarse grinding, oxygen plasma etching, and precisely mechanical polishing were conducted on as-received SCDs. Fig. 11(a) describes the surface after coarse grinding and a wide mechanical scratch exists in the middle of the measurement area. Fig. 11(b) presents the etch pits morphology after oxygen plasma etching and two rough etch pits with layered disordered steps structure dominate the measurement area. Fig. 11(c) and (d) demonstrates the surface of as-received SCD and SCD after precisely mechanical polishing. Obviously, after further mechanical polishing, the mechanical scratches on SCD surface narrowed and the *Sa* roughness decreased. Though the four SCD substrates presented different surface morphology and *Sa* roughness, their surfaces were both smoothed to subnanometer *Sa* roughness after 15 min oxygen plasma treatment at 1000 W RF power. The smoothed surfaces of four different initial SCDs are shown in Fig. 11(e)–(h). The roughness variation of four different initial surfaces is shown in Fig. 11(i). *Sa* roughness of different initial surfaces is 448, 57.7, 2.77, and 1.31 nm, corresponding to coarse grinding treatment, oxygen plasma etching at 600 W RF power, as-received, and precisely mechanical polishing treatment SCDs. After 15 min smoothing, their *Sa* roughness decreases to 0.683, 0.684, 0.548, and 0.465 nm, respectively. Therefore, it is reasonable to conclude that PASE would not depend on the initial surface conditions of SCD. Despite the decreasing trend of *Sa* roughness from coarse grinding to MP treatment after smoothing, all of them remain at the subnanometer level. It is believed that after a sufficient duration of smoothing, the roughness will stabilize at approximately 0.5 nm for all SCDs.

SCD (100) with the dimension of $8 \times 8 \times 0.5$ mm^3 was used to verify the ability of PASE to smooth a larger size of SCD. The as-received SCD was etched by oxygen plasma at 600 W RF power first. Fig. 12(a) and (b) shows the optical images of SCD before and after smoothing. The etched surface of SCD is fuzzy and opaque, and it is hard to see the words behind it. However, after 15 min smoothing, the surface became smooth and quite transparent to see the bottom text. The surface morphology was obtained by AFM and there are 25 images arranged in 5×5 grid. Each image is in the size of 20×20 μm^2 and the center of each image is at the distance of 100 μm when measured. Fig. 12(c) and (d) presents the surface morphology of SCD before and after smoothing. Before smoothing, there were many etch pits on SCD surface and the existence of etch pits caused the rough and blurry surface. The widespread etch pits made the surface height of SCD fluctuate around 600 nm. By contrast, the surface height fluctuation of SCD decreased a hundredfold to 6 nm with a smooth and flat surface after smoothing for 15 min. Fig. 12(e) and (f) demonstrates the specific *Sa* roughness of each AFM image, with Fig. 12(e) corresponding to Fig. 12(c) and Fig. 12(f) corresponding to Fig. 12(d). It is evident that the initial *Sa* roughness of SCD is on the order of tens of nanometers, but after smoothing, SCD achieve a significantly smoother surface with *Sa* roughness at the subnanometer level. Combining the above results, it is reasonable to conclude that PASE is effective to smooth SCD in a large size.

The diamond samples discussed above were all smoothed on (100) crystal plane. Since the quantity and arrangement of carbon atoms vary considerately on different crystal planes which is shown in Fig. 13(a), causing significant differences in polishing characteristics, it is necessary to find out the accessibility of using PASE to smooth SCD with (110) and (111) crystal planes [11]. Here, SCD (110) and (111) with the dimension of $3 \times 3 \times 1$ mm^3 were etched by oxygen plasma at 600 W RF power for 10 min first. The surface morphology of the etched SCD (110) and (111) are shown in Fig. 13(b) and (d), respectively. Interestingly, the etched pits on SCD (110) are similar to cuboids with nearly identical dimensions while the etched surface of SCD (111) presents mountain-like shape in the direction parallel to the image and layered step shape in the direction perpendicular to the image. The corresponding *Sa* roughness of SCD (110) and (111) is 111 nm and 37.5 nm, shown in Fig. 13(f) and (h). After smoothing for 5 min, both the surfaces of SCD (110) and (111) were smoothed, as shown in Fig. 13(c) and (e). The *Sa* roughness decreased to 1.60 nm and 1.80 nm, respectively, which can be seen in Fig. 13(g) and (i).

4. Conclusions

Atmospheric ICP was successfully applied to highly-efficient smoothing of SCD to be subnanometer surface roughness. The smoothing mechanism, surface morphology evolution of SCD were investigated in this paper. Furthermore, analysis on the chemical composition, the removal of damage layer, and the technology applicability of PASE on SCD under various initial conditions was conducted. The following conclusions can be drawn through the above experiment results:

(1) Smoothing of SCD by using atmospheric oxygen plasma is proposed for the first time. The smoothing mechanism, namely PASE, is based on the higher removal priority of carbon atoms with more dangling bonds. During the smoothing process, the

highly reactive oxygen radicals in oxygen plasma would be absorbed on SCD surface and then bond with carbon atoms to form CO/CO_2. Since less C—C bond is required to break for carbon atoms with more dangling bonds, these carbon atoms would have the higher removal priority. Therefore, carbon atoms with different removal priority would be sequentially removed and finally an atom-level smooth surface of SCD with the identical bonding state forms.

(2) The smoothing process is highly affected by the concentration of oxygen reactive radicals and energy input for the reaction system. The study shows that the increase of RF power and flow rate of oxygen would contribute to higher concentration of oxygen active radicals, resulting in a higher MRR. The increase of torch-wafer distance would prolong the contact time between SCD and ambient oxygen, causing unexpected material removal. Furthermore, temperature is a key factor to determine the smoothing effect which can be adjusted by RF power. When RF power reached 900 W, SCD would be smoothed by oxygen plasma, corresponding to the smoothing mode. Higher RF power would bring higher energy input for oxygen dissociation, forming highly active oxygen radicals, and contributing to the breaking C—C bond, so as to achieve SCD smoothing. By adopting proper smoothing conditions, the final *Sa* roughness could stabilize at around 0.5 nm after 5 min smoothing, with a stable MRR of around 20 μm/min, indicating that oxygen plasma possesses the ability to efficiently smooth SCD.

(3) Various characterization methods were utilized to reveal the influence of PASE on SCD surface structure and the chemical composition. The experiment results demonstrate that there was no introduction of damage or impurity during PASE. Meanwhile, the mechanical damage layer and non-diamond composition can be removed by PASE, forming an atomic-scale smooth surface.

(4) SCDs with different initial surface, sizes, and crystal planes were researched to verify the applicability of PASE for SCD under different initial conditions. The experiment results have obviously demonstrated that PASE has no dependence on SCD initial surfaces, sizes, and crystal planes. Therefore, it is reasonable to conclude that PASE is a highly flexible technology for SCD smoothing.

In conclusion, this paper provides a highly-efficient and atomic-scale smoothing method for SCD. The smoothing process can be conducted totally under atmosphere with extensive applicability. The outstanding features of PASE make it a promising technology to achieve atomic-scale manufacturing of SCD in the industry.

CRediT authorship contribution statement

Wang Liu: Validation, Investigation, Data curation. **Yuxi Xiao:** Writing – original draft, Validation, Methodology, Investigation, Data curation. **Yongjie Zhang:** Investigation, Conceptualization. **Quanpeng He:** Writing – review & editing, Supervision. **Hui Deng:** Writing – review & editing, Methodology, Funding acquisition, Conceptualization.

Declaration of competing interest

The authors declare that they have no known competing financial interests or personal relationships that could have appeared to influence the work reported in this paper.

Data availability

Data will be made available on request.

Acknowledgement

This work is supported by the National Natural Science Foundation of China (52375437, 52035009), the Natural Science Foundation of Guangdong Province (2023A1515011461), the Shenzhen Fundamental Research Program (JCYJ20220818100412027) and the Development and Reform Commission of Shenzhen Municipality (F-2023-Z99-503992). The authors acknowledge the assistance of SUSTech Core Research Facilities.

Appendix A. Supplementary data

Supplementary data to this article can be found online at https://doi.org/10.1016/j.diamond.2024.110840.

References

[1] N. Yang, S. Yu, J.V. Macpherson, Y. Einaga, H. Zhao, G. Zhao, G. Swain, X. Jiang, Conductive diamond: synthesis, properties, and electrochemical applications, Chem. Soc. Rev. 48 (1) (2019) 157–204, https://doi.org/10.1039/C7CS00757D.

[2] G. Shu, B. Dai, V.G. Ralchenko, A.P. Bolshakov, A.A. Khomich, E.E. Ashkinazi, J. Han, J. Zhu, Growth of three-dimensional diamond mosaics by microwave plasma-assisted chemical vapor deposition, CrystEngComm 20 (2) (2018) 198–203, https://doi.org/10.1039/C7CE01706E.

[3] H. Hocheng, M.L. Hsieh, Signal analysis of surface roughness in diamond turning of lens molds, Int. J. Mach. Tool Manuf. 44 (15) (2004) 1607–1618, https://doi.org/10.1016/j.ijmachtools.2004.06.003.

[4] K. Harano, T. Satoh, H. Sumiya, Cutting performance of nano-polycrystalline diamond, Diamond Relat. Mater. 24 (2012) 78–82, https://doi.org/10.1016/j.diamond.2011.11.005.

[5] H. Umezawa, Recent advances in diamond power semiconductor devices, Mater. Sci. Semicond. Process. 78 (2018) 147–156, https://doi.org/10.1016/j.mssp.2018.01.007.

[6] T.P. Mollart, C.J.H. Wort, C.S.J. Pickles, M.R. McClymont, N. Perkins, K.L. Lewis, CVD diamond optical components, multispectral properties, and performance at elevated temperatures, SPIE 4375 (2001) 180–198, https://doi.org/10.1117/12.439175.

[7] P.A. Nistor, P.W. May, F. Tamagnini, A.D. Randall, M.A. Caldwell, Long-term culture of pluripotent stem-cell-derived human neurons on diamond–a substrate for neurodegeneration research and therapy, Biomaterials 61 (2015) 139–149, https://doi.org/10.1016/j.biomaterials.2015.04.050.

[8] S. Mandal, E.H.L. Thomas, L. Gines, D. Morgan, J. Green, E.B. Brousseau, O. A. Williams, Redox agent enhanced chemical mechanical polishing of thin film diamond, Carbon 130 (2018) 25–30, https://doi.org/10.1016/j.carbon.2017.12.077.

[9] G. Palasantzas, Random surface roughness influence on gas damped nanoresonators, Appl. Phys. Lett. 90 (4) (2007), https://doi.org/10.1063/1.2435328.

[10] C.M. Flannery, H. Von Kiedrowski, Effects of surface roughness on surface acoustic wave propagation in semiconductor materials, Ultrasonics 40 (1–8) (2002) 83–87, https://doi.org/10.1016/S0041-624X(02)00095-1.

[11] T. Schuelke, T.A. Grotjohn, Diamond polishing, Diamond Relat. Mater. 32 (2013) 17–26, https://doi.org/10.1016/j.diamond.2012.11.007.

[12] M.P. Hitchiner, E.M. Wilks, J. Wilks, The polishing of diamond and diamond composite materials, Wear 94 (1) (1984) 103–120, https://doi.org/10.1016/0043-1648(84)90169-8.

[13] T. Jin, M. Ma, B. Li, Y. Gao, Q. Zhao, Z. Zhao, J. Chen, Y. Tian, Mechanical polishing of ultrahard nanotwinned diamond via transition into hard sp^2-sp^3 amorphous carbon, Carbon 161 (2020) 1–6, https://doi.org/10.1016/j.carbon.2020.01.041.

[14] A.P. Malshe, B.S. Park, W.D. Brown, H.A. Naseem, A review of techniques for polishing and planarizing chemically vapor-deposited (CVD) diamond films and substrates, Diamond Relat. Mater. 8 (7) (1999) 1198–1213, https://doi.org/10.1016/S0925-9635(99)00088-6.

[15] A. Kubota, S. Nagae, S. Motoyama, High-precision mechanical polishing method for diamond substrate using micron-sized diamond abrasive grains, Diamond Relat. Mater. 101 (2020) 107644, https://doi.org/10.1016/j.diamond.2019.107644.

[16] Z. Yuan, Z. Jin, Y. Zhang, Q. Wen, Chemical mechanical polishing slurries for chemically vapor-deposited diamond films, J. Manuf. Sci. Eng. 135 (4) (2013) 041006, https://doi.org/10.1115/1.4024034.

[17] L. Liao, Z. Zhang, F. Meng, D. Liu, B. Wu, Y. Li, W. Xie, A novel slurry for chemical mechanical polishing of single crystal diamond, Appl. Surf. Sci. 564 (2021) 150431, https://doi.org/10.1016/j.apsusc.2021.150431.

[18] Y. Chen, L.C. Zhang, J.A. Arsecularatne, C. Montross, Polishing of polycrystalline diamond by the technique of dynamic friction, part 1: prediction of the interface temperature rise, Int. J. Mach. Tool Manuf. 46 (6) (2006) 580–587, https://doi.org/10.1016/j.ijmachtools.2005.07.018.

[19] Y. Chen, L.C. Zhang, J.A. Arsecularatne, I. Zarudi, Polishing of polycrystalline diamond by the technique of dynamic friction, part 3: mechanism exploration through debris analysis, Int. J. Mach. Tool Manuf. 47 (15) (2007) 2282–2289, https://doi.org/10.1016/j.ijmachtools.2007.06.004.

[20] Y. Chen, L.C. Zhang, Polishing of polycrystalline diamond by the technique of dynamic friction, part 4: establishing the polishing map, Int. J. Mach. Tool Manuf. 49 (3–4) (2009) 309–314, https://doi.org/10.1016/j.ijmachtools.2008.10.010.
[21] Y. Chen, W. Liu, H. Feng, L. Zhang, Failure mechanisms of CVD diamond wafers and thin films during polishing, Mach. Sci. Technol. 19 (1) (2015) 152–173, https://doi.org/10.1080/10910344.2014.991030.
[22] F. Tang, Y. Chen, L. Zhang, Analysis of polished polycrystalline diamond using dual beam focused ion beam microscopy, Philos. Mag. 92 (13) (2012) 1680–1690, https://doi.org/10.1080/14786435.2012.657706.
[23] H. Liu, L. Xie, W. Lin, M. Hong, Optical quality laser polishing of CVD diamond by UV pulsed laser irradiation, Adv. Opt. Mater. 9 (21) (2021) 2100537, https://doi.org/10.1002/adom.202100537.
[24] B. Yan, N. Chen, N. He, Y. Wu, X. Zhang, L. Li, Surface modeling and component analysis of picosecond laser ablation of CVD diamond, Diamond Relat. Mater. 111 (2021) 108191, https://doi.org/10.1016/j.diamond.2020.108191.
[25] Z. Fang, Y. Zhang, R. Li, Y. Liang, H. Deng, An efficient approach for atomic-scale polishing of single-crystal silicon via plasma-based atom-selective etching, Int. J. Mach. Tool Manuf. 159 (2020) 103649, https://doi.org/10.1016/j.ijmachtools.2020.103649.
[26] W.B. Jung, S. Jang, S.Y. Cho, H.J. Jeon, H.T. Jung, Recent progress in simple and cost-effective top-down lithography for ≈10 nm scale nanopatterns: from edge lithography to secondary sputtering lithography, Adv. Mater. 32 (35) (2020) 1907101, https://doi.org/10.1002/adma.201907101.
[27] W. Guo, S.K. Anantharajan, X. Zhang, H. Deng, A study on the damage layer removal of single-crystal silicon wafer after atmospheric-pressure plasma etching, J. Micro Nano-Manuf. 8 (2) (2020) 024501, https://doi.org/10.1115/1.4046377.
[28] S.J. Ullal, H. Singh, J. Daugherty, V. Vahedi, E.S. Aydil, Maintaining reproducible plasma reactor wall conditions: SF_6 plasma cleaning of films deposited on chamber walls during Cl_2/O_2 plasma etching of Si, J. Vac. Sci. Technol. A 20 (4) (2002) 1195–1201, https://doi.org/10.1116/1.1479733.
[29] L. Zhang, B. Wu, Y. Zhang, H. Deng, Highly efficient and atomic scale polishing of GaN via plasma-based atom-selective etching, Appl. Surf. Sci. 620 (2023) 156786, https://doi.org/10.1016/j.apsusc.2023.156786.
[30] S.-G. Ri, H. Watanabe, M. Ogura, D. Takeuchi, S. Yamasaki, H. Okushi, Hydrogen plasma etching mechanism on (001) diamond, J. Cryst. Growth 293 (2006) 311–317, https://doi.org/10.1016/j.jcrysgro.2006.05.036.
[31] H. Kuroshima, T. Makino, S. Yamasaki, T. Matsumoto, T. Inokuma, N. Tokuda, Mechanism of anisotropic etching on diamond (111) surfaces by a hydrogen plasma treatment, Appl. Surf. Sci. 422 (2017) 452–455, https://doi.org/10.1016/j.apsusc.2017.06.005.
[32] L. Xie, T.X. Zhou, R.J. Stöhr, A. Yacoby, Crystallographic orientation dependent reactive ion etching in single crystal diamond, Adv. Mater. 30 (2018) 1705501, https://doi.org/10.1002/adma.201705501.
[33] H. Luo, K.M. Ajmal, W. Liu, K. Yamamura, H. Deng, Atomic-scale and damage-free polishing of single crystal diamond enhanced by atmospheric pressure inductively coupled plasma, Carbon 182 (2021) 175–184, https://doi.org/10.1016/j.carbon.2021.05.062.
[34] N. Tsubouchi, Y. Mokuno, S. Shikata, Characterizations of etch pits formed on single crystal diamond surface using oxygen/hydrogen plasma surface treatment, Diamond Relat. Mater. 63 (2016) 43–46, https://doi.org/10.1016/j.diamond.2015.08.012.
[35] S. Ghodbane, D. Ballutaud, F. Omnès, C. Agnès, Comparison of the XPS spectra from homoepitaxial {111},{100} and polycrystalline boron-doped diamond films, Diamond Relat. Mater. 19 (5–6) (2010) 630–636, https://doi.org/10.1016/j.diamond.2010.01.014.
[36] J.B. Wu, M.L. Lin, X. Cong, H.N. Liu, P.H. Tan, Raman spectroscopy of graphene-based materials and its applications in related devices, Chem. Soc. Rev. 47 (5) (2018) 1822–1873, https://doi.org/10.1039/C6CS00915H.
[37] V. Thapliyal, M.E. Alabdulkarim, D.R. Whelan, B. Mainali, J.L. Maxwell, A concise review of the Raman spectra of carbon allotropes, Diamond Relat. Mater. 127 (2022) 109180, https://doi.org/10.1016/j.diamond.2022.109180.